Science Advances

AAAS

advances.sciencemag.org/cgi/content/full/3/8/e1700672/DC1

Supplementary Materials for

Observation of prethermalization in long-range interacting spin chains

Brian Neyenhuis, Jiehang Zhang, Paul W. Hess, Jacob Smith, Aaron C. Lee, Phil Richerme, Zhe-Xuan Gong, Alexey V. Gorshkov, Christopher Monroe

Published 25 August 2017, *Sci. Adv.* **3**, e1700672 (2017)
DOI: 10.1126/sciadv.1700672

This PDF file includes:

Experimental noise sources and their influence on the thermalization dynamics

As discussed in the text, there are fluctuations on the interaction strength J_{ij}, which originate from noise on the laser intensity and ω_m [39]. This noise is slow compared to a single experiment, but fast compared to the thousands of experiments it takes to complete a data set. Averaging over this classical noise leads to dynamics that resemble a running time average, because the fast temporal oscillations are effectively canceled out by the fluctuating J_{ij}. To account for this, the numeric simulations average over a small range of coupling strengths (standard deviation of $0.12 J_{\max}$).
Another source of noise is the fourth order AC Stark shift from the Mølmer-Sørensen interaction laser sidebands. This noise also has a negligible effect, since we are in the regime of large transverse fields and this Stark shift term only adds a small global σ_z fluctuation of about 30 Hz, on top of the 10 kHz transverse field applied. We experimentally verify this by applying a global offset field of $\pm$ 400 Hz and observe no difference in the observed prethermalization. The relaxation dynamics are robust against these experimental noise sources, however it is sensitive to asymmetries of the spin-spin coupling matrix.

Measuring the spin-spin coupling matrix

We directly measure the spin-spin coupling matrices for seven ions for both long and short range interactions and ensure it is symmetric as seen in fig. S1. In order to measure the strength of the interaction between two spins, we shelve all but the two ions of interest out of the interaction space and directly observe their time evolution. This is done by first performing individual rotations on these two ions to the $|\uparrow\rangle_z$ as outlined above. Then we perform a global π rotation between $|\downarrow\rangle_z$, $^2\mathrm{S}_{1/2}|F=0, m_F=0\rangle$, and one of the Zeeman states, $^2\mathrm{S}_{1/2}|F=1, m_F=-1\rangle$, which takes the other 5 spins out of the interaction space. We then apply the Hamiltonian which now only acts on the two remaining spins.

Justification for postselection

As noted above the initial N spin flip fidelity is approximately $(0.97)^N$ and $(0.85)^N$ for short and long range interactions respectively. Numerically, we find that the number of spin excitations is essentially constant on the experimental timescale which is expected because the transverse field Ising model can be mapped to an XY model for sufficiently large transverse field and the XY model conserves the number of spin excitations [33]. However, experimentally we observe leakage out of the N excitation subspace with less than 50% remaining at the end of the evolution. This leakage error is largely due to the residual spin-phonon entanglement ignored in Eq. 1 and that extra spin excitations can be created by phonons within our experimental time scale. For clarity, we postselect the data for the correct number of spin excitations

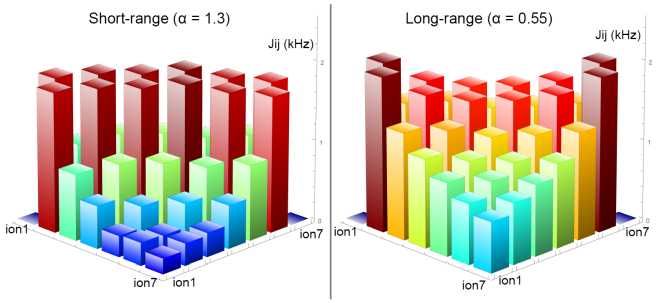

fig. S1. We directly measure the spin-spin coupling matrix with seven ions for both short-range (left matrix) and long-range (right matrix) interactions and see it is symmetric. To measure the coupling between two spins we transfer all except the spins of interest out of the interaction space. This is done by shelving the other spins in one of the Zeeman levels. The estimated statistical error on J_{ij} is 10% on the nearest-neighbour coupling strengths.

to eliminate the effects of imperfect state preparation, detection error, and small deviations from our model Hamiltonian due to unwanted excitations of the phonon modes.

The spin-boson mapping and the generalized Gibbs ensemble

To explain our observed prethermalization, it is convenient to map the spins into bosons by using the Holstein-Primakoff transformation: $\sigma_i^z = 2a_i^\dagger a_i - 1$, $\sigma_i^+ = a_i^\dagger \sqrt{1 - a_i^\dagger a_i}$. We will assume that the average spin excitation density $\bar{n} = \sum_i \langle a_i^\dagger a_i \rangle / N$ is much smaller than 1. This assumption is justified in our experiments because our initial states have small spin excitation densities and we set $\max(J_{ij}) \ll B$ so the amount of $\bar{n}$ that will be dynamically created is small [$\sim (\max(J_{ij})/B)^2$]. Therefore to the lowest order we can approximate $\sigma_i^+ \approx a_i^\dagger$, and (1) reduces to an integrable Hamiltonian H_0 made of non-interacting bosons

$$H_0 = \sum_{i<j} J_{ij}(a_i^\dagger a_j + a_i^\dagger a_j^\dagger + h.c.) + 2B \sum_i a_i^\dagger a_i \qquad (1)$$

$$H_1 = H - H_0 \qquad (2)$$

Here H_1 contains interactions between the bosons which are parametrically small in $\bar{n}$, and, as a result, we can treat H_1 as a perturbation to H_0. Thus, it is natural to expect the system (in the thermodynamic limit) to first relax to a prethermal state described by the GGE of H_0, and to later relax to a thermal state described by the full H. Naively, we expect the thermalization to happen at a time scale much longer than the relaxation to GGE, based on the different energy scales of H_0 and H_1. However, this is not always the case, as discussed below. To explicitly define the GGE of H_0, we would need to first diagonalize H_0 and find the integrals of motion. Note that (1) only involves J_{ij} for $i < j$. For convenience, we will define a new matrix $\mathcal{J}$ such that $\mathcal{J}_{ii} = 0$ and $\mathcal{J}_{ij} = \mathcal{J}_{ji} = J_{ij}$ for

$i < j$. H_0 can be rewritten as

$$H_0 = \sum_{i,j} \mathcal{J}_{ij} \left[a_i^\dagger a_j + \frac{1}{2}(a_i^\dagger a_j^\dagger + a_i a_j) \right] + 2B \sum_i a_i^\dagger a_i \quad (3)$$

An orthogonal matrix $\mathcal{V}$ can be used to diagonalize the matrix $\mathcal{J}$ as $\sum_{i,j} \mathcal{V}_{ik} \mathcal{J}_{ij} \mathcal{V}_{jk'} = \nu_k \delta_{kk'}$, where $\{\nu_k\}$ are the eigenvalues of matrix $\mathcal{J}$. Introducing $c_k = \sum_i \mathcal{V}_{ik} a_i$, we have

$$H_0 = \sum_k \left[(\nu_k + 2B) c_k^\dagger c_k + \frac{1}{2} \nu_k (c_k^\dagger c_k^\dagger + c_k c_k) \right] \quad (4)$$

Next, we perform a Bogoliubov transformation $c_k = \cosh(\theta_k) d_k - \sinh(\theta_k) d_k^\dagger$ with $\theta_k = \frac{1}{2} \tanh^{-1}(\frac{\nu_k}{\nu_k + 2B})$ to fully diagonalize H_0

$$H_0 = \sum_k \epsilon_k d_k^\dagger d_k, \quad \epsilon_k \equiv 2\sqrt{B(B + \nu_k)} \quad (5)$$

Since integrable models have an extensive number of conserved quantities that are not taken into account by canonical ensembles from statistical mechanics, the GGE was developed to make predictions about equilibrium values of observables in these systems by incorporating the additional integrals of motion [14-18]. The GGE for H_0 is defined as

$$\rho_{GGE} = \frac{e^{-\sum_k \lambda_k d_k^\dagger d_k}}{\mathrm{Tr}(e^{-\sum_k \lambda_k d_k^\dagger d_k})} \quad (6)$$

with λ_ks determined by $\langle d_k^\dagger d_k \rangle_0 = \langle d_k^\dagger d_k \rangle_{GGE}$, where the notation $\langle \cdots \rangle_0$ denotes the expectation value in the initial state $|\psi_0\rangle$, and the notation $\langle \cdots \rangle_{GGE}$ denotes the expectation value in ρ_{GGE}. We observe relaxation to the GGE if for any local observable O, $\langle O(t) \rangle \approx \mathrm{tr}(O \rho_{GGE})$.

Using the fact that our initial state $|\psi_0\rangle$ is always a Fock state in the basis of $\{a_i^\dagger a_i\}$, the value of $\langle d_k^\dagger d_k \rangle_0$ can be calculated by the following formula

$$\langle d_k^\dagger d_k \rangle_0 = \cosh(2\theta_k) \sum_i \mathcal{V}_{ik}^2 \langle a_i^\dagger a_i \rangle_0 + \sinh^2(\theta_k) \quad (7)$$

To calculate the expectation values of $\sigma_i^z = 2 a_i^\dagger a_i - 1$ in the GGE, we use the following equations

$$\begin{aligned} \langle a_i^\dagger a_i \rangle_{GGE} &= \langle \sum_{k,k'} \mathcal{V}_{ik} \mathcal{V}_{ik'} c_k^\dagger c_{k'} \rangle_{GGE} \\ &= \sum_k \mathcal{V}_{ik}^2 \langle \cosh(2\theta_k) d_k^\dagger d_k + \sinh^2(\theta_k) \rangle_{GGE} \\ &= \sum_k \mathcal{V}_{ik}^2 [\cosh(2\theta_k) \langle d_k^\dagger d_k \rangle_0 + \sinh^2(\theta_k)] \end{aligned} \quad (8)$$

where we use the fact that ρ_{GGE} is diagonal in the Fock basis of $\{d_k^\dagger d_k\}$, so $\langle d_k^\dagger d_{k'} \rangle_{GGE} = \langle d_k^\dagger d_{k'}^\dagger \rangle_{GGE} = 0$ for $k \neq k'$.

Single-particle properties of H_0

Since v_k/B is small, we can expand ϵ_k and d_k in ν_k/B to the leading order

$$\epsilon_k \approx 2B + \nu_k, \quad d_k \approx \sum_i \mathcal{V}_{ik} (a_i + \frac{\nu_k}{4B} a_i^\dagger) \quad (9)$$

This means to understand the single-particle properties of H_0 (Eq. 5), we just need to understand the properties of the eigenvalues $\{\nu_k\}$ and eigenvectors $\mathcal{V}$ of the matrix $\mathcal{J}$. We emphasize that the matrix J defined in Eq. 3 of the main text differs from the matrix $\mathcal{J}$ used in defining H_0, because $J_{ii} \neq 0$ by the above definition . This is because J_{ii} has no physical consequence in the Ising Hamiltonian as $(\sigma_i^x)^2 = 1$.

Let us first try to understand the properties of the eigenvalues and eigenvectors of the matrix J. To make this possible, we will need to approximate the spacing between ions to be uniform. While this is not true in the current experiment due to the harmonic trapping potential, the inhomogeneity in ion spacing is not responsible for the observed prethermalization [20] and from now on we will assume that the ions are equally spaced.

We now write down the motional Hamiltonian of N ions trapped along the z direction ignoring the ions' motion along the y direction for simplicity since we barely couple the spins to the phonons in that direction

$$H_m = \sum_{i=1}^N \left[\frac{p_{i,x}^2}{2M} + \frac{p_{i,z}^2}{2M} + V(z_i) + \frac{1}{2} M \omega_x^2 x_i^2 \right] \quad (10)$$

$$+ \frac{Q^2}{4\pi\epsilon_0} \sum_{i=1}^N \sum_{j=1}^{i-1} \frac{1}{\sqrt{(z_i - z_j)^2 + (x_i - x_j)^2}} \quad (11)$$

Here $\{x_i, z_i, p_{i,x}, p_{i,z}\}$ are respectively the coordinates and momenta of the i^{th} ion in the x and z directions. M and Q are the mass and charge of each ion, and ω_x is the transverse trapping frequency. The ions will be equally spaced with a spacing a_0 if $V(z) = -\frac{Q^2}{4\pi\epsilon_0 a_0} \log(1 - z^2/L^2)$, with $L = N a_0/2$.

By expanding the Coulomb interaction around the ions' equilibrium positions up to second order in position, the motional Hamiltonian in the x direction can be written as

$$H_{mx} = \sum_{i=1}^N \frac{p_{i,x}^2}{2M} + \frac{1}{2} M \left(\sum_{i=1}^N \omega_x^2 x_i^2 - \omega_z^2 \sum_{i,j=1}^N K_{ij} x_i x_j \right) \quad (12)$$

where we have set $\omega_z \equiv \sqrt{\frac{Q^2}{4\pi\epsilon_0 M a_0^3}}$ as an "effective" axial trapping frequency. The dimensionless matrix K characterizes the *dipolar interactions* between ions

$$K_{i \neq j} = -|i - j|^{-3}, \quad K_{ii} = -\sum_{j \neq i} K_{ij} \quad (13)$$

The exact analytical expressions for the eigenvalues $\{\kappa_m\}$ and eigenvectors $\{V_{i,m}\}$ of K cannot be obtained. But we can employ a first-order perturbation theory and assume that

the eigenvectors of K are approximately the same as those of a nearest-neighbor coupling matrix K. As a result

$$V_{i,m} \approx \begin{cases} \sqrt{1/N}, & m = 0, \\ \sqrt{\frac{2}{N}} \cos[\frac{m\pi}{N}(i-\frac{1}{2})], & m = 1, 2, \cdots N-1 \end{cases} \quad (14)$$

$$\kappa_m \approx \sum_{r=1}^{N/2} \frac{2 - 2\cos\frac{mr\pi}{N}}{r^3}, \quad (m = 0, 1, \cdots N-1) \quad (15)$$

Note that the $(i-\frac{1}{2})$ above ensures that the phonon modes are either symmetric or antisymmetric under the spatial inversion of the chain ($i \to N+1-i$).

As a result, the eigenvectors of the matrix J are given by $\{V_{i,m}\}$, and the eigenvalues are given by

$$\lambda_m = \frac{\hbar(\delta k)^2 \Omega^2}{2M(\mu^2 - \omega_x^2 + \omega_z^2 \kappa_m)} \quad (16)$$

Finally, we point out that importantly, J_{ii} is in general non-uniform. This can be seen in the following two limits:

1. When $\mu^2 - \omega_x^2 \gg \omega_z^2 \kappa_m$ for all m, we expect J_{ij} to decay as $1/|i-j|^3$ ($\alpha \to 3$ limit), and

$$J_{ii} \approx \frac{\hbar(\delta k)^2 \Omega^2 \omega_z^2}{2M(\mu^2 - \omega_x^2)^2} K_{ii} \quad (17)$$

   J_{ii} in this limit is very close to uniform in the large N limit, except for i close to 1 and N [see fig. S2(a)].

2. When $\mu^2 - \omega_x^2 \ll \omega_z^2 \kappa_m$ for all $m \neq 0$ ($\alpha \to 0$ limit), we can separate out the $m = 0$ term and approximate J_{ii} by

$$J_{ii} \approx \frac{\hbar(\delta k)^2 \Omega^2}{2M\omega_z^2} \frac{1}{N} \left\{ 1 + 2 \sum_{m=1}^{N-1} \frac{\cos^2[\frac{m\pi}{N}(i-\frac{1}{2})]}{\kappa_m} \right\} \quad (18)$$

   Note that even in the large N limit, J_{ii} is non-uniform across the entire ion chain [see fig. S2(a)]. An analytical formula can be obtained if we approximate κ_m by including only the $r = 1$ (nearest-neighbor) term in Eq. 15, leading to $J_{ii} \approx \frac{\hbar(\delta k)^2 \Omega^2}{2M\omega_z^2} \frac{1}{N}(i - \frac{N+1}{2})^2 +$ constant.

As shown above, when the interactions described by J_{ij} are very long-ranged, J_{ii} can be rather non-uniform. This will result in a qualitatively different structure between the eigenvalues and eigenvectors of the two matrices J and $\mathcal{J}$. To see this, we first notice that the eigenvalues and eigenvectors of J are similar to those of the Hamiltonian for a free-particle in an square well potential. This connection can be formalized by going into the continuum limit and introducing a continuous momentum $q \equiv m\pi/N \in (0, \pi)$. The eigenspectrum $\lambda(q)$ of J is minimized at $q = \pi$. Expanding $\lambda(q)$ around $q = \pi$ and using Eq. 15-16, we obtain

$$\lambda(q) \approx O((q-\pi)^0) + \frac{\hbar(\delta k)^2}{2M_{\text{eff}}}(q-\pi)^2 + O[(q-\pi)^4] \quad (19)$$

$$M_{\text{eff}} \equiv M \frac{\left[\mu^2 - \omega_x^2 + 4\zeta(3)\right]^2}{\omega_z^2 \Omega^2 \ln 2} \quad (20)$$

corresponding to the dispersion relation of a massive particle with an effective mass M_{eff} and an effective momentum $(\delta k)q$. Here we point out that because the low-energy spin waves have momentum around $q = \pi$, the long-range hoppings among local spin excitations are canceling out each other and do not lead to non-analytic dispersion relation, thus the spin-wave approximation remains valid as in a short-range interacting transverse-field Ising model.

The Schrödinger equation for the above particle can be written in the position space parameterized by a continuous coordinate $z \in [1, N]$ that replaces the discrete ion index $i \in \{1, 2, \cdots N\}$

$$-\frac{\hbar^2(\delta k)^2}{2M_{\text{eff}}} \frac{\partial^2}{\partial z^2} \psi(z) = E\psi(z) \quad (21)$$

with the boundary condition $\psi(z \leq 1) = \psi(z \geq N) = 0$ corresponding to that of a particle in a box potential. Here the eigenwavefunction $\psi_m(z) \approx (-1)^i V_{i,m}$ (for $z = i$), and the eigenenergy $E_m \approx \hbar\lambda_m$ (up to a constant shift) near $q = \pi$.

We can similarly map the eigenvalue equation of $\mathcal{J}$ to a Schrödinger equation of a massive particle

$$-\frac{\hbar^2(\delta k)^2}{2M_{\text{eff}}} \frac{\partial^2}{\partial z^2} \Psi(z) + U(z) = \mathcal{E}\Psi(z) \quad (22)$$

However, we now have an effective potential $U(z)$ due to the fact that $\mathcal{J}_{ii} = 0 \neq J_{ii}$, and up to a constant energy shift

$$U(z) \equiv \begin{cases} \infty & z < 1 \text{ or } z > N \\ -J_{ii} & z = i \in \{1, 2, \cdots, N\} \end{cases} \quad (23)$$

As discussed in the previous section, for $\mu^2 - \omega_x^2 \gg \omega_z^2 \kappa_m$ (where $\alpha \to 3$), the potential $U(z)$ will be nearly flat, and the eigenvalues and eigenvectors of $\mathcal{J}$ are similar to those of a particle in a box. However, for $\mu^2 - \omega_x^2 \ll \omega_z^2 \kappa_m$ (where $\alpha \to 0$), $U(z)$ has the shape of a double well potential [fig. S2(a)].

Discussion

Ignoring tunneling between the two deep wells of a double-well-shaped potential, the low-energy eigenstates of a massive particle in such a potential are localized orbitals inside either well [see fig. S2(b)]. The tunneling rate (which is exponentially small in the height of the barrier) splits the degeneracy of the localized orbitals in each well and leads to pairs of symmetric and antisymmetric (upon the spatial inversion of the chain) wavefunctions. This physical picture explains the observed prethermalization: Initial excitations placed in the left half of the chain will be localized for an extended period of time under the evolution of H_0, until the tunneling between the two wells eventually delocalizes the excitations. The explicit scaling of the tunneling rate as a function of α and system size N is difficult to obtain and requires future theoretical study, due to the challenge in obtaining an analytical solution to Eq. 22 for a given α.

Although the physics we observe is similar to weakly interacting bosons in a double-well potential, it is important to

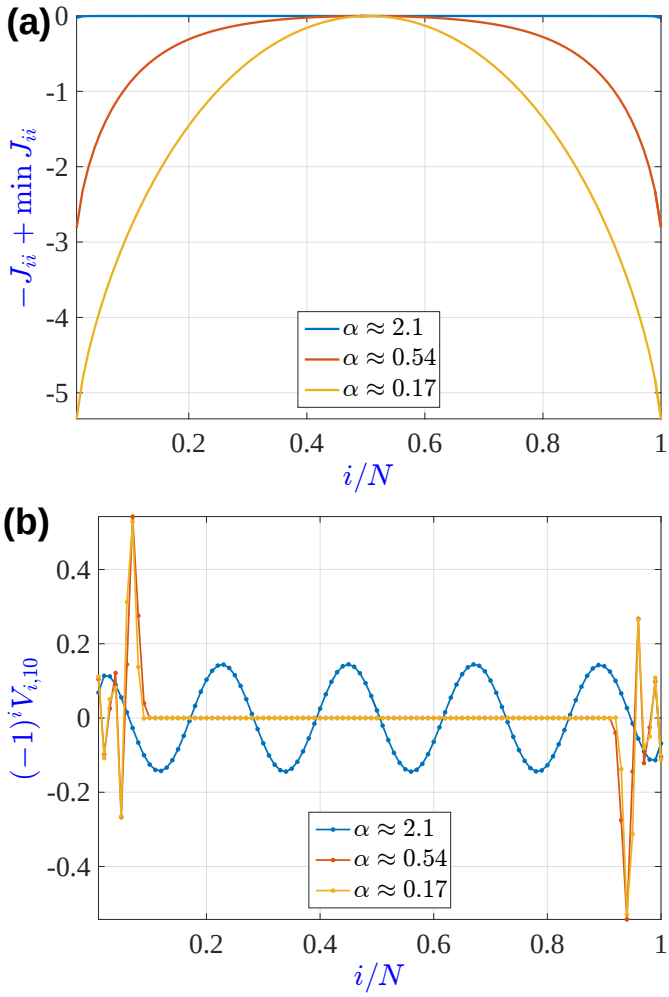

fig. S2. Numerical calculation to illustrate the origin of the double-well potential.
(a) The diagonal matrix element $-J_{ii}$ [in arbitrary units and shifted by $\min(J_{ii})$] that determines the single-particle potential $U(z)$ for $N = 100$ ions. We choose the parameters that make J_{ij} decay approximately as $1/r^{\alpha}$ with different values of α shown in the plot. As α decreases, the potential changes continuously from nearly flat to an approximately harmonic anti-trap. Together with two hard wall potentials at $i/N = 0, 1$, the potential looks like a double well that becomes deeper for smaller α. (b) The eigenvector $V_{i,10}$ corresponding to the 10^{th} lowest eigenvalue of $\mathcal{J}$ for a $N = 100$ ion chain. For small α's, the eigenvector, as well as the wavefunction $\Psi(z)$ of Eq. 22, is localized inside the two wells. For large α's, the eigenvector is delocalized and similar to that of a particle in a box.

emphasize that, in our system, the double-well potential is not present in the Hamiltonian H_0 (Eq. 1). Instead, the effective potential emerges from the long-range hoppings of the bosons with open boundary conditions. This emergent inhomogeneous potential is a particularly surprising effect because the motional Hamiltonian (Eq. 11) and spin-motion couplings induced by the Raman lasers are all homogeneous. The key reason is that for a short-range interacting system, translational invariance can usually be assumed for an open boundary chain as far as bulk properties are concerned. But long-range interactions make the boundary conditions important even for bulk properties, which is why spin excitations in the bulk can still feel a strongly inhomogeneous potential. Finding the critical α at which this effect takes place in our system is still an open question, because it is difficult to find the analytical expression for J_{ii} as a function of α.

The notion of a boundary starts to break down for sufficiently long-ranged interactions, and therefore we cannot attribute the observed prethermalization to boundary effects. Usually, boundary effects only affect a finite number of eigenstates and do not affect local quenches in the bulk. However, here there is an extensive number of eigenstates that are localized in the two wells because the width of the wells is proportional to the chain length [see fig. S2(a)], and excitations placed an extensive number of lattice sites away from the edges are still subject to the quantum tunneling effect.

Finally, we point out that interactions in H_1 can also delocalize the initial spin excitations placed in one of the wells, and eventually thermalize the system. As a result, there is an interesting interplay between the timescales of prethermalization to the GGE and of thermalization. If the interactions in H_1 are sufficiently weaker than the kinetic tunneling rate in H_0, which can be achieved by increasing the magnetic field strength B or changing the range of interactions, then we expect the system to have two prethermal phases before thermalization, with the observed prethermalization followed by prethermalization to the GGE of H_0. If instead the tunneling rate is sufficiently smaller than the interactions in H_1, then the prethermal states described by the GGE of H_0 may never appear during the time evolution. These interesting multi-stage relaxation processes will require future experimental investigations with longer coherence times and larger spin chains.